ELSEVIER

Journal of Power Sources 110 (2002) 330–340

JOURNAL OF POWER SOURCES

www.elsevier.com/locate/jpowsour

Advanced integrated battery testing and simulation

Bor Yann Liaw*, Keith P. Bethune, Xiao Guang Yang

Hawaii Natural Energy Institute, SOEST, University of Hawaii at Manoa, 2540 Dole Street, Holmes Hall 246, Honolulu, HI 96822, USA

Abstract

The recent rapid expansion in the use of portable electronics, computers, personal data assistants, cellular phones, power tools, and even electric and hybrid vehicles creates a strong demand on fast deployment of battery technologies at an unprecedented rate. To facilitate such a development integrated battery testing and simulation (IBTS) using computer modeling is an effective tool to improve our capability of rapid prototyping battery technology and facilitating concurrent product development. In this paper, we will present a state-of-the-art approach to use IBTS for improvements in battery cell design, operation optimization, and even charge control for advanced batteries.

Keywords: Integrated battery testing and simulation; Electric and hybrid vehicles; Computer modeling; Battery design; Charge control

1. Introduction

In the last decade, the development of electric and hybrid vehicles and the rapid expansion of portable computers, consumer electronics and telecommunication tools in the US and other regions of the world have sparked an enormous interest in developing advanced battery systems for high-power applications. These developments called for rapid prototyping of batteries and devices integration, better charging and safety control, and long-lasting cycle life. To satisfy these demands and needs, conventional technology and product developments have to incorporate more innovative capabilities to meet the challenges and requirements.

The problem the battery industry faces today is that there is essentially no effective tool to help them develop the products in a timely manner. We should realize that laboratory testing and benchmarking can only provide a certain level of competency to understand battery performance under a controlled condition, but in no way to extrapolate the results to field applications, where the operating environment is hardly controlled. Therefore, the battery performance is unpredictable in real-life situations due to the sporadic and unconditioned nature of the operating conditions and user habits. We, therefore, conceive that a tangible approach that can extend the laboratory and controlled testing to field applications is to combine the laboratory testing and computer simulation to develop a tool that can predict and model real-life battery behavior in a comprehensive manner. With this tool, battery performance can be understood and predicted in details. With this tool, we can hasten product design and development, derive sensible operating conditions to enhance device performance and safety, optimize charging and discharging control to extend the battery life, and allow system integration with advanced CAD/CAM tools in concurrent manufacturing facility, so the design and manufacturing capability in the battery industry will be greatly enhanced.

Such an integrated battery testing and simulation (IBTS) approach needs to meet the following criteria to make it viable in practical applications:

1. The tool must be comprehensive and flexible enough to cover a wide range of engineering prototyping and performance requirements.
2. The computation must be effective and efficient enough that the prediction and validation can be accomplished in a timely manner.
3. The capability must be cost effective and time saving.
4. The model and tools must be knowledge-based, built on fundamental principles and basic understanding of the chemistry; therefore can be repeatedly used for the same chemistry without serious modifications from time to time. Thus it is robust and long-lasting for technology transfer.

In this paper, we would like to discuss the status of computational battery simulation capability, particularly focus on the modeling approach from ''first-principles'',

* Corresponding author. Tel.: +1-808-956-2339; fax: +1-808-956-2335.
E-mail address: bliaw@hawaii.edu (B.Y. Liaw).

0378-7753/02/$ – see front matter
PII: S0378-7753(02)00195-7

which we believe, provide the best possibility to meet the above requirements.

Modeling and simulating battery performance from "first-principles" is a viable approach, which can provide a significant amount of detailed information on battery behaviors to allow us understand battery characteristics and optimize its performance. Successful battery modeling efforts from "first-principles" have been reported in the past by a few laboratories [1–7]. We will not repeat the model development here. Interested readers should refer to these earlier works for further information on respective modeling principles and capabilities.

What will be focused in this paper is to utilize a recently developed multiphase, electrochemical–thermal coupled model [5–7] and some practical examples to illustrate the capabilities and benefits of the computational modeling and assess the future directions in this approach. For example, we believe that high-power rapid charging technology is an important aspect in making battery applications more readily accessible and reliable. We will devote a significant portion of the discussions to show how an integrated battery development and simulation approach can assist us understand rapid charging limiting mechanism in valve-regulated lead–acid (VRLA) [8] and nickel–metal hydride (Ni–MH) [9] systems and help us improve battery design and charging strategy for rapid charging performance and sustain battery cycle life. We found that taking this IBTS approach with detailed validation can be a powerful and effective R&D tool for battery technology development.

2. The numerical model and simulation

Detail descriptions of the formulation of the simulation model and the numerical approach are reported in [5–7] and will not be repeated here. Only a brief description is provided here to give an overview of the model and procedures. The numerical model is built on our understanding of the physical model of the battery chemistry and typical cell configuration including geometry, microstructure, and individual component composition. The "first-principle" model incorporates microscopic electrode reactions, such as those usually depicted by Butler–Volmer equations for charge transfer part and phase transformation rate equations for species transfer part; and transport phenomena, often in porous media, as described by typical diffusion, migration and advection equations, into a homogeneous but coupled numerical framework and then solves these partial differential equations (PDEs) to obtain numerical solutions for the potential and concentration profiles of the active species as a function of time and space distribution. By formulating the microscopic reaction and transport equations in a representative volume within a macroscopic framework and using a volume averaging method we were able to simplify the numerical computation steps but still obtain accurate enough detail numerical solutions of the system. We can further incorporate coupled electrochemical and thermal behaviors in the same homogeneous body and solve the governing equations by the same single PDE solver simultaneously to obtain temperature dependent information. The coupling of the electrochemical and thermal phenomena is essential to proper description of the mass transport and charge transfer behaviors in the system, since they are often thermally activated and therefore sensitive to temperature excursions. The numerical approach and computational procedures are based on proprietary computational fluid dynamics (CFD) techniques. Fig. 1 shows the overall schematic of the numerical model approach and predictive capability.

3. Experimental aspects

A viable battery modeling and simulation is characterized by how well the model can be validated. It is therefore critical for us to demonstrate good agreement between detailed experimental validation and model prediction. In order to do so, we need to control the test conditions in the most reliable and comprehensive way to produce validation

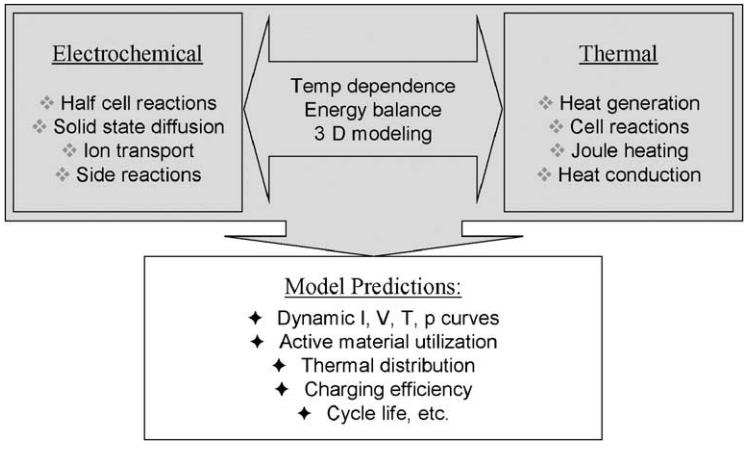

Fig. 1. Schematic of the battery model framework showing coupled electrochemical and thermal phenomena in a battery system and the model capability.

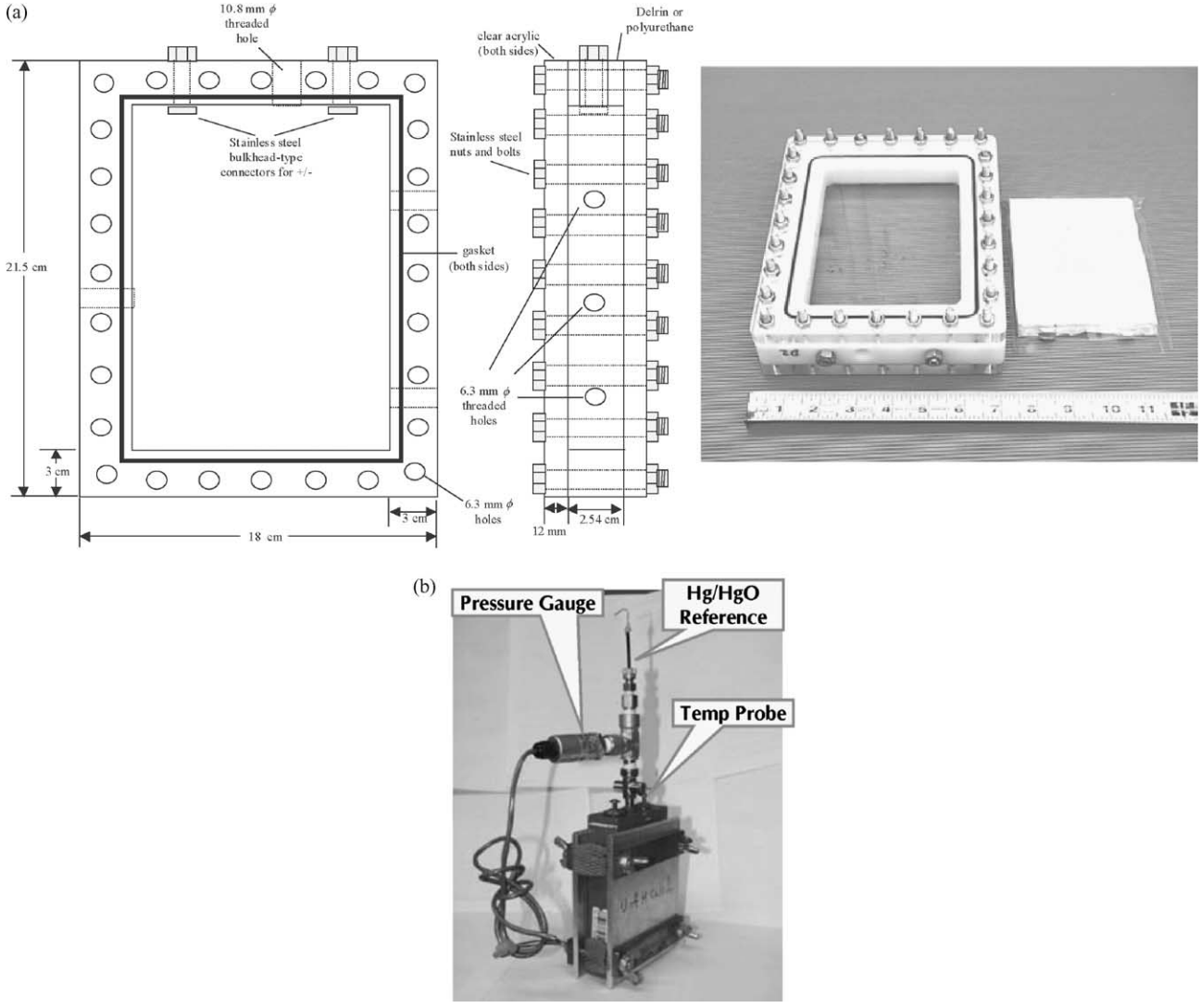

Fig. 2. Test cells for (a) VRLA and (b) Ni–MH systems.

results. And, we have to construct controllable single test cells to conduct reliable and reproducible experiments. Thus, we often have to construct test cells from scratch with green electrode plates and separators provided by a manufacturer and form the cells accordingly. This is done for most of our VRLA work. On the other hand, for Ni–MH cells, we often have to rely on the manufacturer to construct the test cells for us according to experimental requirements. Fig. 2 shows the test cells for (a) VRLA and (b) Ni–MH systems that were used in this work for validations and detailed characterizations.

Fig. 2a shows the test apparatus including the VRLA test cell. The test apparatus has two compartments: a smaller one resides inside with carefully machined dimensions and fixtures to secure the cell compression and provide a constant volume for accurate acid saturation control and an outer one with fixtures to provide gas tight seal, support posts for electrical connection, and house adaptors for temperature and pressure probe installations. The cell design allows the electrode potentials, internal cell temperature, and gas pressure being monitored simultaneously and recorded for testing and simulation validation.

Fig. 2b shows the Ni–MH test cell from a manufacturer, resembling a commercial configuration with a standard Hg/HgO reference electrode installed to monitor individual electrode behaviors. The cell also comes with a gas release valve that can be used to install an adaptor for gas pressure gauge attachment. Thermocouples were also used in the external walls of the cell for temperature measurements. Therefore, the cell and electrode potential, current, temperature and gas pressure can be recorded and correlated simultaneously, providing necessary information for detail validation.

For electrochemical investigations, two types of battery test equipment were used. One is an Arbin BT-2043 battery test station, which has four high-current channels each with a 20 ADC and 20 VDC range and four low-current channels with the same voltage range but only have 2 ADC for the

current range. The Arbin machine was used for cell tests in the low power range. When the power level required for the test was higher than that which Arbin machine can handle, an AeroVironment ABC-150 battery cycler was used. The ABC-150 battery cycler can handle power up to 120 kW or current up to 256 ADC per channel.

4. Results and discussion

Fig. 3 shows acid concentration distributions in lead–acid batteries to illustrate the capability of the simulation in providing detailed information of battery's performance. Fig. 3a shows the acid concentration profiles as a function of charge time determined along the plate height in a flooded configuration where acid stratification is important to the cell performance. Fig. 3b shows the acid concentration profiles as a function of charge time determined along the length of the cell in a VRLA configuration. Both figures demonstrated that detailed acid concentration can be estimated as a function of time and space distribution in both flooded and valve-regulated configurations, which can assist us understand battery performance during a progression of a charge reaction when experimental data might not be readily available or difficult to obtain at the same time. This type of information certainly is very useful in battery design and development.

Similarly, another example is shown in Fig. 4 to illustrate that the simulation is capable of predicting dynamic battery performance, such as in charge–discharge cycles or other dynamic test regimes. Fig. 4 illustrates a nominal 6.5 Ah 7.2 V Ni–MH module tested under a constant-current discharging and charging cycle and followed by a dynamic stress test (DST). In all three regimes, the simulation results consistently predict the battery performance with excellent agreement. With such agreement, we believe that the model and simulation can predict battery behavior in real-life situations quite reliably, therefore effectively assisting the battery engineers to develop better understanding of the battery performance.

There are a few benefits from this practice that uses the integrated testing and dynamic simulation capabilities. For example, the physical dimensions of the cell can be easily changed, and performance simulated, so the dimensions can be optimized for the best performance. The optimization can minimize the waste of active materials and increase utilization efficiency. In addition, the same approach can be used to study the limiting factors in a "what if" situation. For example, we can study the performance characteristics if the cell design is limited by either the negative or positive electrode capacity and understand what the impact is from the respective limitation. The same characterization can be used to estimate the operating limitation of the battery and the underlying limiting mechanism. These simulations can be further tested and verified by constructing prototypes to validate the simulation results. Above these significant benefits, one of the most important aspects of this approach is that the simulation, as presented here in Fig. 3 or Fig. 4, can be carried out in a short period of computation time, as short as 1/100th of the duration for the actual test. Thus, it is not only cost effective but also time saving, a true advancement in technology development.

In the following section, we will illustrate two practical examples of how to use the integrated testing and simulation to assist the development of rapid charging techniques for VRLA and Ni–MH systems, respectively.

In the example of the VRLA system, the work presented here will focus on how to use the simulation capability to examine various possible design factors that could limit the transport phenomenon under constant-current rapid charge conditions in a VRLA cell. Due to limited space, we will present only a few key parameters to illustrate significant features in the discussion. We will not be able to discuss the

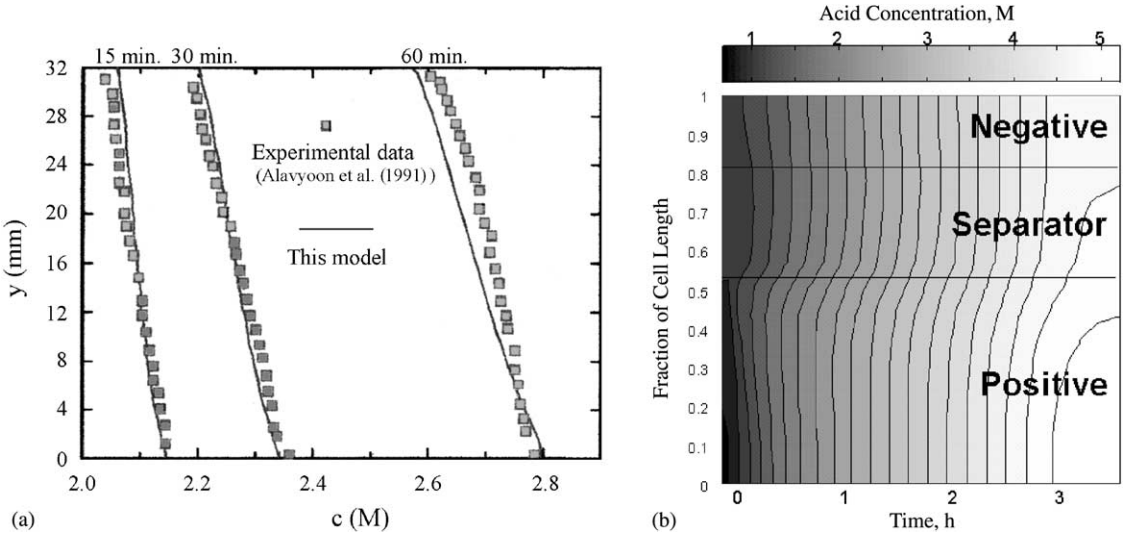

Fig. 3. Acid concentration profiles of (a) flooded and (b) valve-regulated configurations during charging. The spatial and time resolutions are shown.

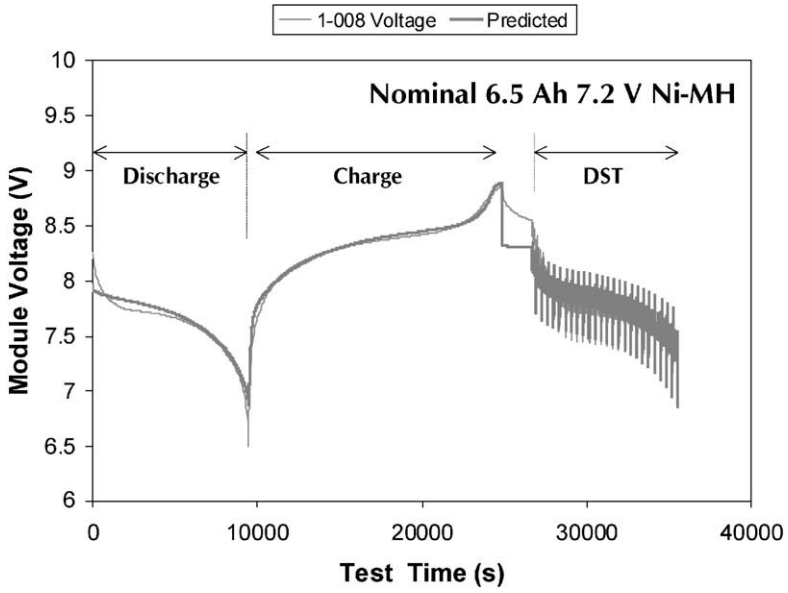

Fig. 4. A discharge, charge and DST test cycle of a nominal 6.5 Ah 7.2 V Ni–MH module with simulation results showing excellent agreement.

experimental validation aspects (to be published elsewhere), where the cells have to be tested under a variety of charging rates and compared with the simulation. To aid the discussion, it should be noted that the cell is positive (P) limiting with a single cell made of one positive (P) plate sandwiched with two negative (N) plates in a N–P–N configuration. We also overcharged the cell to collect information in the overcharge regime. On the other hand, the test cell capacity was estimated by the negative plate, thus the discharge regime tends to overdischarge the positive plate, which caused acid depletion as we observed in the test results later.

Fig. 5 shows the parameters that are important to the test control and validation. Among them, the saturation level is probably the most important one but also one of the most difficult to control. We found that careful control of the saturation level is the key to reproduce the results and obtain excellent agreement with the simulation.

Fig. 6 shows good agreement of a typical *C*/3 constant-current charge regime of the test cell, as illustrated by the recorded (solid lines) and predicted (dash lines) cell voltage and pressure profiles. It should be noted that, upon charging, the cell voltage displayed an initial overshoot and followed by a brief voltage relaxation before showing the gradual polarization voltage increase, implying that, at this rate, the acid depletion does exist. On the other hand, the acid depletion had no impact on the pressure profile which showed a smooth decline in the first 2.5 h before the gas evolution became noticeable and accelerated at the end of the charge. It should be noted that the final pressure buildup was dominated by hydrogen evolution.

As we further compare the charge performance at high rates, as shown in Fig. 7, for 2 and 3 C charge regime, respectively, the agreement is consistent as well. As the charge rate went up, so did the polarization potential; the 3 C test terminated earlier with the same voltage cut-off. To our surprise, the pressure profiles in the two tests were very similar, implying that the same gas reaction was taking place and the gassing rate was independent of the charge rate. Further analysis [8] showed that transport of acid is the rate limiting factor and contributes significantly to the cell polarization potential and the acid depletion in the positive plate. On the other hand, the charge transfer impedance for

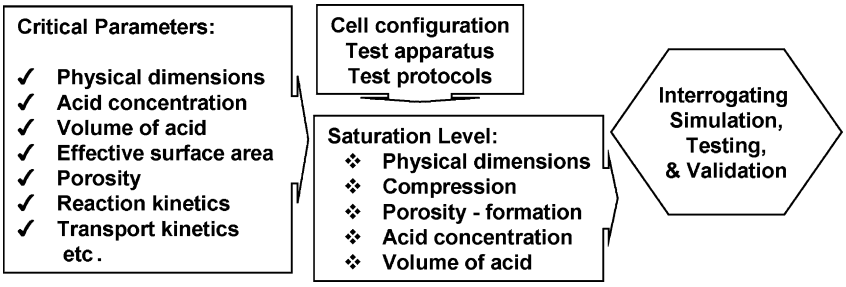

Fig. 5. A schematic showing the control issues in the experiments, including the consideration of critical parameters in the design of the test cell configuration and the control of the saturation level in the cell.

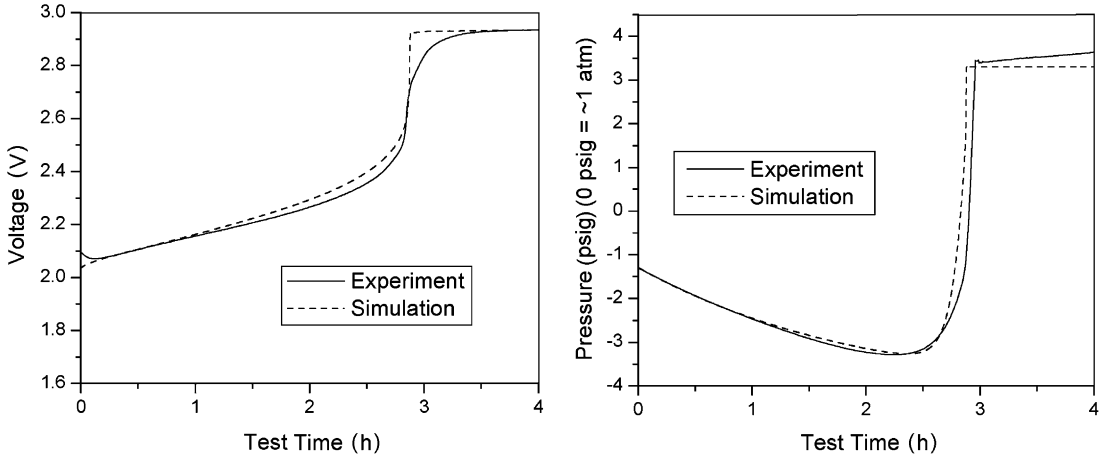

Fig. 6. Cell voltage and pressure profiles of a test cell under *C*/3 charge regime. Considerable overcharge is shown with venting of the gas after 3 h into the charge. Good agreement is shown between the experimental data and the simulation results.

sulfation and gas reactions are negligible, thus almost independent of the charge rate.

As the transport of the acid, as well as the gas transport in the absorptive glass mat (AGM) separator, may well be the rate limiting process for rapid charging, it is important to know how the cell metrics affect the charge performance. Simulation becomes a very handy and powerful tool for this purpose.

Fig. 8a shows how the acid saturation level affects the charge performance. With an electrolyte-starving cell of three different saturation levels, we found that at 70% saturation, the acid starvation in the positive electrode led to the initial voltage overshoot and relaxation. If the saturation level was over 85%, the starvation and the initial voltage overshoot and relaxation would disappear. In contrast, the influence on the polarization potential was indistinguishable. On the other hand, the impact on the pressure profile is noticeable; the higher the saturation level, the more severe the pressure buildup. The pressure buildup potentially would result in unwanted venting and dry-out from the loss of electrolyte.

Fig. 8b illustrates the influence of the cell geometry. The simulation shows that as the electrode thickness reduced by half, the cell is less vulnerable to the polarization of the acid concentration at high rates. The more sustainable acid distribution eliminated the acid depletion even at 70% saturation, thus the cell can be charged at a more aggressive rate with a more gradual increase in the polarization potential than in the original configuration. The reduction in polarization will also lessen the pressure development during charging.

The last point that worth mentioning is the influence of the porosity of the electrode plates on the charge performance. Fig. 9a and b show the influences from negative and positive electrode, respectively. Fig. 9a indicates that, as the porosity of the Pb negative plate increases, the morphology change reduces the effective surface area, thus increases the polarization current density, resulting in enhanced gassing and pressure buildup. The impact on the cell voltage is however complex due to the fact that the cell voltage is supposedly determined predominantly by the positive plate, while the

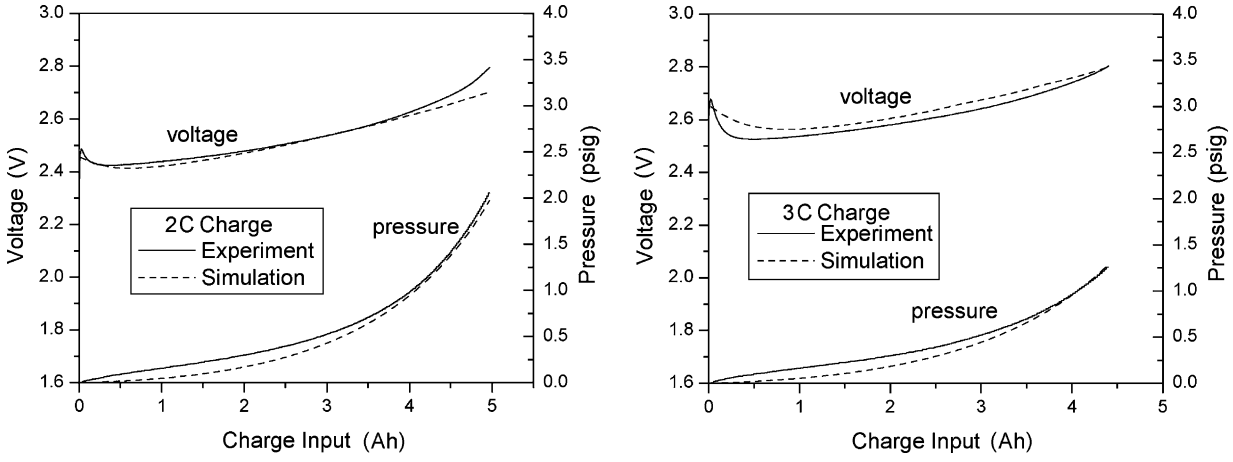

Fig. 7. Comparison of rapid charging performance at high rates between experimental results and simulation predictions. Both cell voltage and pressure profiles are shown. Good agreement is observed.

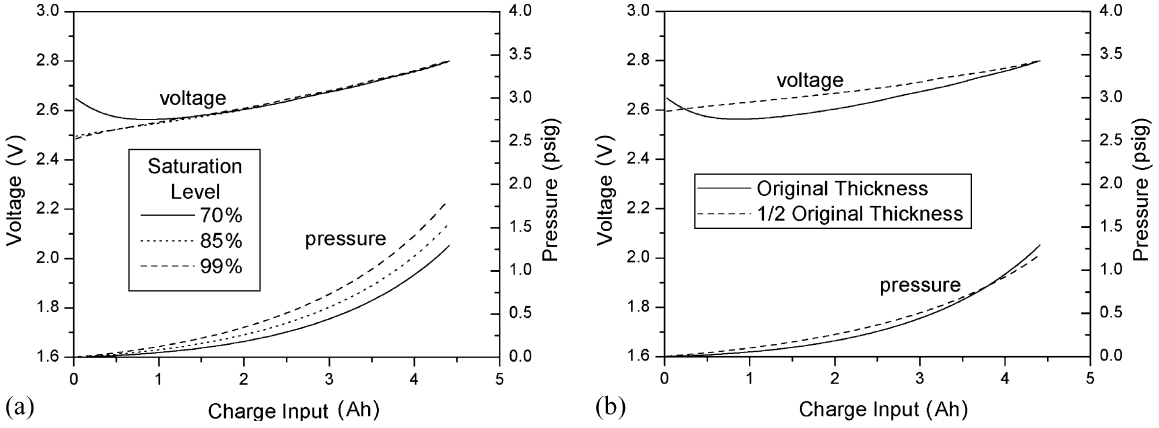

Fig. 8. Impacts of cell performance from cell metrics, such as the acid saturation level and plate thickness variation.

porosity change in the negative plate does affect the transport behavior of the cell and the positive electrode potential. Fig. 9b, in contrast, shows that the increase in porosity in the positive plate can alleviate the acid depletion, while the influence on gassing is minimal. The porosity increase assists the acid transport in the pores of the positive plate, thus reduces the acid depletion. The gassing behavior, on the other hand, is determined by the negative plate, thus reflecting a negligible impact from the positive plate.

In the next example, we will focus our discussion on the rapid charging mechanistic study of the Ni–MH system, particularly how modeling of the hydrogen concentration via the simulation can help us identify the limiting mechanism in such a charging process and develop a sensible strategy for improvement in the cell design.

Fig. 10 displays the most significant features in charging Ni–MH modules with high rate charging, which show that the pressure increases exponentially with the charge input in each respective charging regime. The rapid increase of the pressure dictates that the charging control should be dominated by the pressure termination. This important parameter of pressure control becomes the most critical aspect and the limiting factor in the charge return of the battery. Therefore, understanding the underlying process of the pressure buildup is crucial for cell design and for improving charge performance under high rates.

To understand the gassing process and the kinetics involved, we have to seek a more detailed analysis of the gassing reaction mechanism from both experimental evidence and numerical simulation. The first step has to rely on additional experimental evidence to identify the limiting reaction. The test cell, as shown in Fig. 2b, was used to monitor the individual electrode behavior and correlate the potential change with pressure profile to find out which electrode and gas species were responsible for the pressure buildup. Fig. 11 shows the electrode potential changes during the high rate charging for Ni and MH electrode, respectively. The results indicate that the potential change on the Ni was not sufficient to distinguish what reaction and gas species were involved. In contrast, the MH electrode potential depicted some interesting features that can be used to trace what was happening in the cell.

It should be noted that other in situ measurements [10] have been conducted in the cell to characterize the thermodynamic and kinetic properties of the individual electrodes. Information obtained from that study [9,10], including the hydrogen diffusion coefficient and the ohmic and charge transfer resistance values, enabled us to identify the reaction

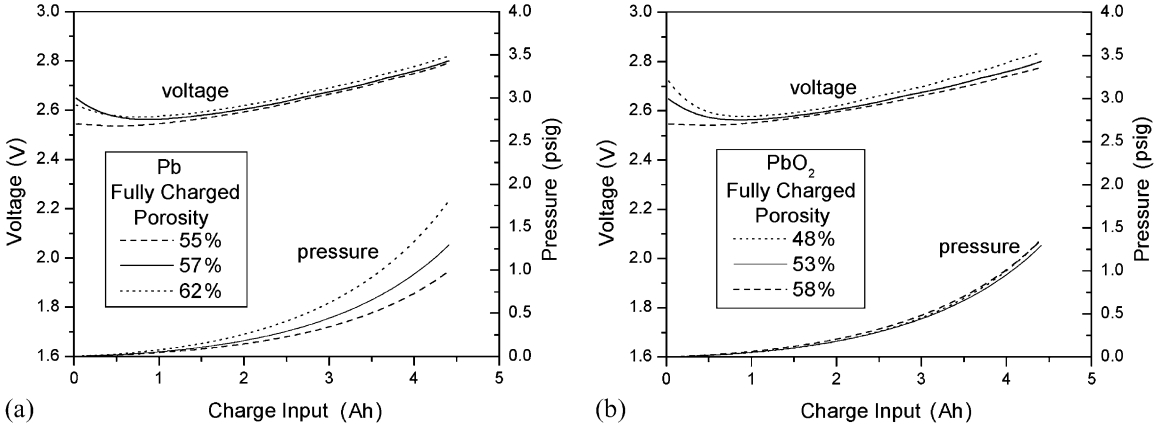

Fig. 9. Influence of the electrode porosity on the cell rapid charge performance.

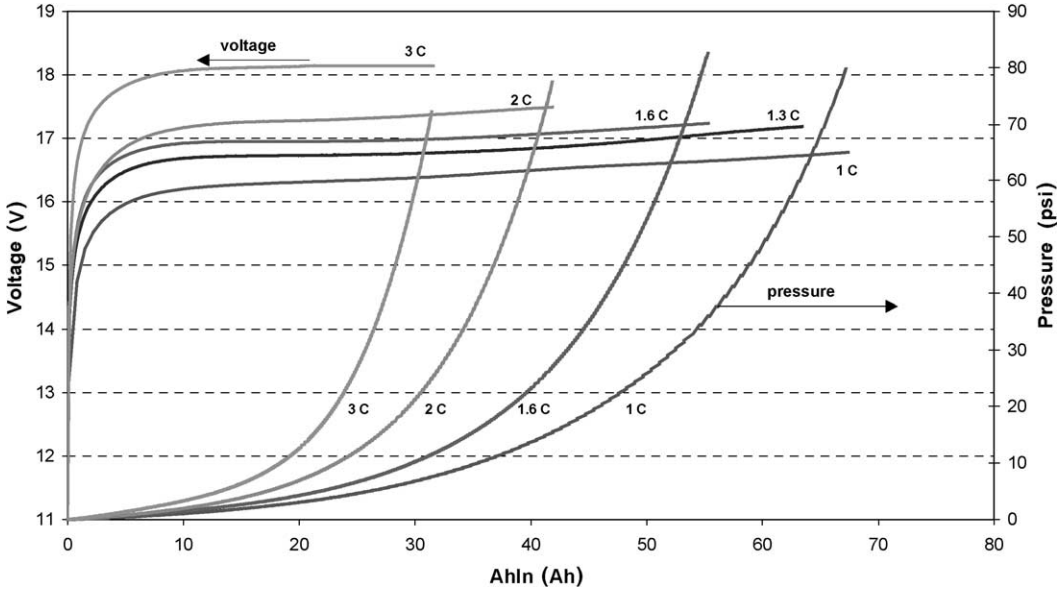

Fig. 10. Voltage and pressure profiles of a Ni–MH module tested under various rapid charging regimes.

mechanism of the gas evolution. For example, the resistance values measured from the IR voltages indicated that the primary contribution is from the MH electrode, suggesting that the electrode transport is an issue. Additional analysis from linear cyclic micro-polarization led to the conclusion that the charge transfer resistance is negligible in the MH electrode; thus, the transport-related resistance is the major contribution to the gas reaction impedance.

The potential excursions, as shown in Fig. 11, and their correlation with the pressure profiles, as shown in Fig. 10, are essential and important to the understanding of what gas evolution reactions are involved at high rate charging. The figure shows that as the charging progresses, the MH electrode potential was polarized to a more negative direction, while the Ni electrode potential moved in the opposite direction. The polarization potential increased with the charge rate in each electrode. As explained previously in [11], we can interpret the potential excursions as follows. First, as the Ni electrode was polarized at high rates, the oxygen evolution took place in an early stage, most likely during the first 5–8 Ah of the charge input. The progressing recombination of oxygen was signaled by the change of the MH electrode potential toward a more positive direction, and a minimum around 10 Ah of charge input was observed. Subsequently, as the hydrogen insertion into the MH alloy became less efficient, hydrogen evolution gradually became dominant as indicated by the increasing polarization toward a more negative direction now in the MH electrode potential. The accompanying pressure increase suggested that the hydrogen evolution was responsible for the pressure buildup in the cell.

To further understand the hydrogen transport process in the cell, especially through the MH electrode interface and in the bulk, and to elucidate the limiting process that impedes the overall transport property in the charge regime, a mathematical model and simulation was employed. A schematic describing the mathematical model for the hydrogen transport analysis is shown in Fig. 12, in which we concentrated on the MH electrode and the electrolyte inter-

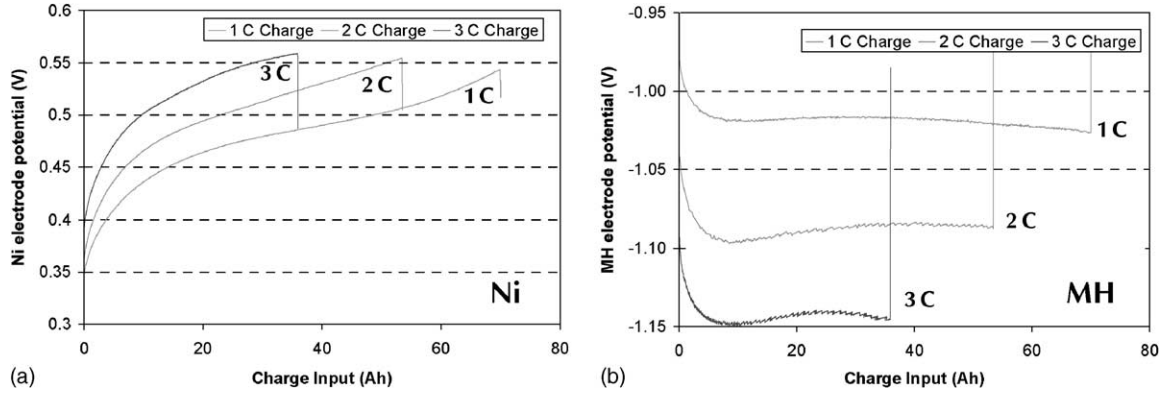

Fig. 11. Individual electrode potential change during high rate charging for (a) Ni and (b) MH electrode, respectively, vs. a standard Hg/HgO.

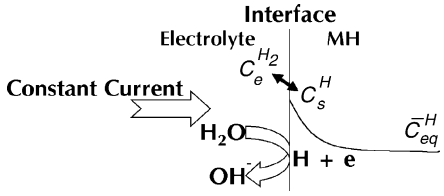

Fig. 12. A schematic description of a mathematic model for the hydrogen transport process involved in the Ni–MH system.

face. Under a constant-current condition, a constant flow of hydrogen species is imposed on the MH surface where the charge transfer reaction taking place as:

$$H_2O + e^- = OH^- + H_{ad} \quad (1)$$

The adsorbed hydrogen, H_{ad}, can undergo two branches of reactions; namely, via a "spill-over" step and become an absorbed hydrogen in the bulk as:

$$H_{ad} + M = MH_{ab} \quad (2)$$

or combine with a nearby hydrogen species and become a hydrogen gas molecule, often staying on the surface as an adsorbed species.

$$H_{ad} + H_{ad} = H_{2(g)} \quad (3)$$

Reactions (2) and (3) are competing reactions often co-exist in the MH systems. Reaction (2) is kinetically more favorable than (3), whereas thermodynamically it is the opposite. We assume that reaction (2) will establish a surface hydrogen concentration, C_s^H, in the solid phase of the MH framework in reference to the MH bulk, where a finite equilibrium bulk hydrogen concentration, $\bar{C}_{eq}^H$, exists in the core. Reaction (3) will result in a hydrogen molecule concentration in the electrolyte, represented by $C_e^{H_2}$, depending on the solubility of hydrogen in the electrolyte solution. The concentration gradient imposed by the charging process will drive the solid-state diffusion of hydrogen inwards, and there is a quasi-equilibrium between the surface hydrogen concentration in the solid phase and the hydrogen concentration in the electrolyte solution at the interface. The solid-state diffusion can be solved using a typical diffusion PDE described by Crank [12] directly, or by numerical model computation, with proper initial and boundary conditions. Fig. 13 shows the result from the numerical computation. Interestingly, if we trace the surface hydrogen concentration profiles with the charge time for various rates, as shown in Fig. 14A, we found that the duration for the surface hydrogen concentration to reach the maximum hydrogen content in the MH is very similar to the charge time determined in the experiments at various charge rates. This analysis suggests that the charge regime was limited by the solid-state hydrogen diffusion in the MH. Again, the results of this analysis are consistent with the observations on the ohmic and polarization impedance behaviors from the IR voltage analysis and the linear cyclic micro-polarization experiments, of which the transport-related impedance is the major contribution to the reaction resistance.

With the understanding of the limiting mechanism in the rapid charge process of the Ni–MH system, we were now able to conduct further analysis regarding some cell design specifics to improve the charge performance of the system. For example, Fig. 15a illustrates that improvement of the solid-state hydrogen diffusion can significantly enhance the charge performance; thus, seeking a better MH with a higher diffusivity can be part of the solution. On the other hand, Fig. 15b indicates that reducing MH particle size could have a profound effect on the charge performance with the same MH composition. The particle size effect was actually verified via a comparison with other Ni–MH systems of smaller particle sizes, supporting our analysis that the charge performance could be drastically improved by the proposed particle size reduction.

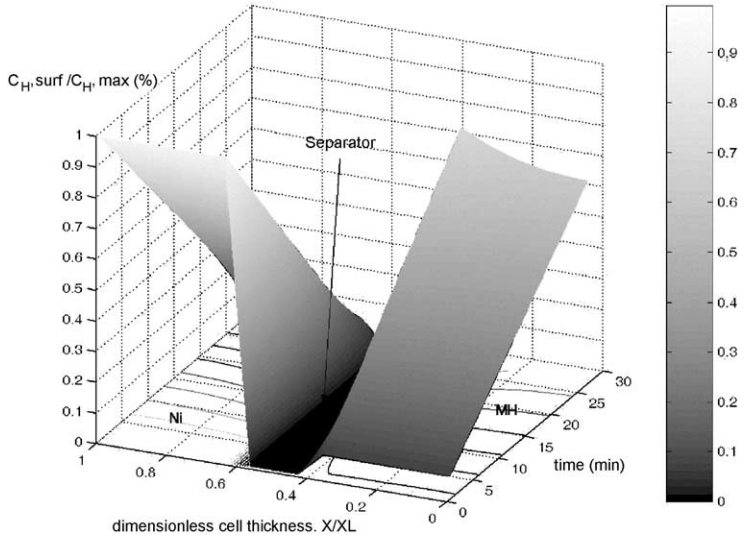

Fig. 13. Concentration profiles of hydrogen species in the electrodes during charging as a function of charge time and cell dimension.

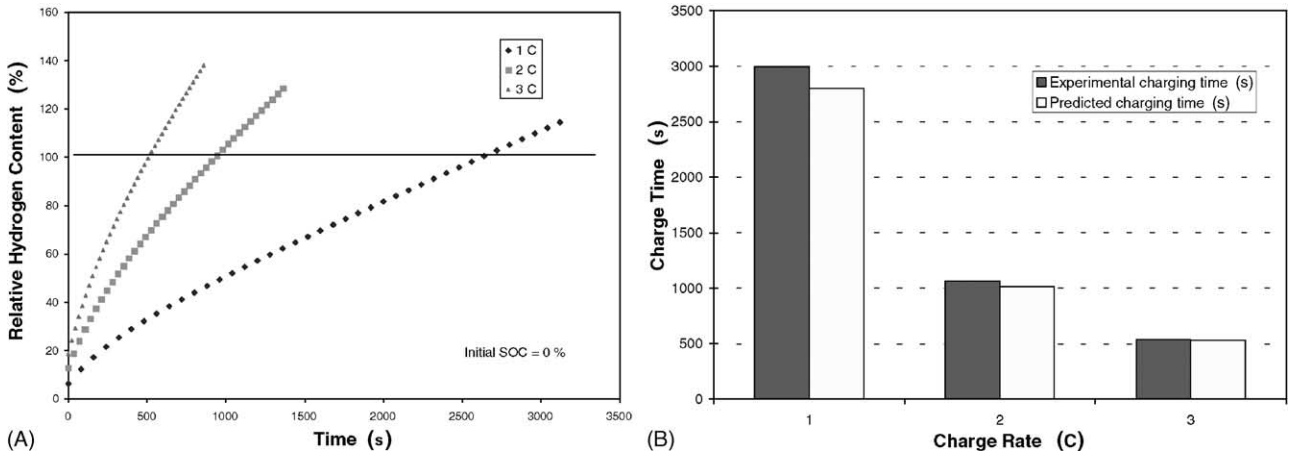

Fig. 14. (A) Surface hydrogen concentration profiles as a function of charge time at various charge rates. (B) Comparison of the duration of which the surface hydrogen concentration reaches the maximum content with the experimental charge time for each charge rate in three rapid charge regimes.

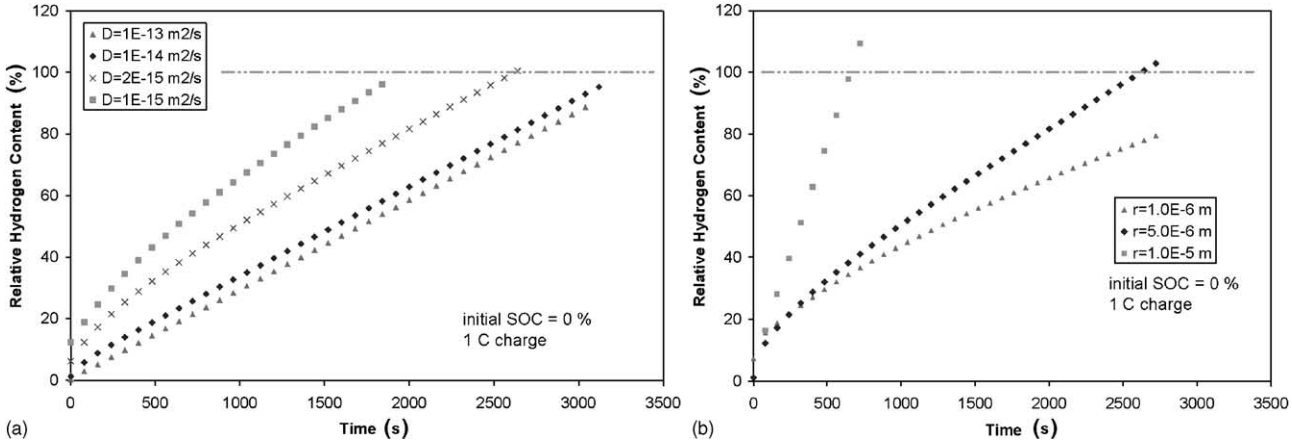

Fig. 15. Analyses of charge performance of the Ni–MH battery system with variations in (a) solid-state hydrogen diffusion in the MH and (b) MH particle size under 1 C rate. Under an ideal situation, the cell should return to full capacity at 1 C in 3600 s. The charge time for each profile to reach 100% relative hydrogen content vs. 3600 s specifies the percentage of charge return.

The successful application of the IBTS approach with the powerful and cost effective modeling tool paved a way for advanced battery research and development, as shown in the above examples in the VRLA and Ni–MH systems. The applications of this unique approach to other chemistries have been demonstrated recently as well, although not in as much details as the examples shown here. Therefore, we believe that IBTS can expedite advanced battery developments in pace with the demands in rapid battery prototyping and system integration and make substantial contributions.

5. Future directions

A few highlights we think are worth mentioning here. We are currently using the IBTS approach to study battery cycle life, in an attempt to predict battery life under various duty cycles. In order to predict the cycle life, degradation mechanisms have to be identified, characterized and quantified and then incorporated into the model to simulate the degradation processes incurring during the duty cycles. This is an overwhelming and challenging effort, but promising great payoffs. One serious problem with the current battery modeling lies on the fact that the simulation cannot predict battery performance over the life, where degradation does occur. Our effort will shed some lights on what the critical issues are and how coupled degradation mechanisms can be validated properly so high fidelity predictions can be accomplished. The multitude in the experimental efforts for validation is certainly overwhelming, but not insurmountable. Good progress is being made, and the initial results are encouraging.

Another area that promises great payoffs is the extension of the ‘‘first-principle’’ models to include adaptive intelligence using fuzzy and neural network approach to train and develop suitable algorithms to predict battery performance in dynamic field conditions. The combined capability of the ‘‘first-principle’’ model and the adaptive approach can provide the best prediction and control tool in the field applications, for the use in charge control, optimization of

power use of the battery pack in hybrid configurations, or solving other system development and integration issues. We are currently using this approach to analyze vehicle battery pack performance in field testing and the result is very promising.

The computational efficiency of our current simulation code is quite impressive. For example, for a typical model simulation of a power duty cycle (charging, discharging, DST or any dynamic conditions), the computation time on a typical PC workstation is about 1/10th to 1/100th of the actual process duration, depending on the complexity of the cycle. Therefore, the technique can be used in a real-life situation to conduct almost real-time prediction in a practical and realistic time scale. Of course, further improvements on the computation power, algorithm, efficiency, and more detailed understanding of the battery performance issues will enhance the capability and accuracy (fidelity) of the prediction.

6. Conclusion

Our approach of using IBTS with detailed interrogative experimental validation can provide a powerful and effective R&D tool for battery technology development. This tool can be applied to almost every aspect and stage of the battery design, development, operation, and system integration. We have used both VRLA and Ni–MH systems to demonstrate the effectiveness and usefulness of this IBTS approach. As the VRLA and Ni–MH systems remain competitive in power source and energy storage applications, we believe that an effective use of this tool can substantially improve the battery performance and reliability.

On a side issue, the rapid charging techniques can present significant benefits and create positive impacts on the battery performance and cycle life. We showed that both types of battery can be recharged at high rates reliably, although the cycle life issue needs more detailed validation. We believe that we have captured in-depth understanding of the battery charge performance characteristics, and such understanding is the key to enable battery to perform successfully in field applications. The rapid charging process in both systems seems to be limited by the transport process in the cell. Battery charge performance can be optimized through proper cell design, processing, and charge control.

Acknowledgements

The authors would like to thank U.S. Department of Defense, Defense Advanced Research Projects Agency (DARPA), and Hawaii Electric Vehicle Demonstration Project (HEVDP) for supporting this work under the Federal Cooperative Agreement MDA972-95-0009 and the support from the U.S. Department of Transportation under the Advanced Vehicle Program (AVP), in the Other Transaction Agreement No. DTRS56-99-T-0017. Additional support from Ford Motor Company is highly appreciated. Some useful discussions and technical assistances from Dr. Dennis Corrigan and Ron Brost are also appreciated. The authors would also like to thank Prof. C.Y. Wang and his past and current co-workers at the Pennsylvania State University for their assistance in developing the simulation code, which is critical to the success of this work.

References

[1] J.C. Newman, W. Tiedemann, J. Electrochem. Soc. 144 (1997) 3081.
[2] D.M. Bernardi, M.K. Carpenter, J. Electrochem. Soc. 142 (1995) 2631.
[3] T.V. Nguyen, R.E. White, H. Gu, J. Electrochem. Soc. 137 (1990) 2998.
[4] T.V. Nguyen, R.E. White, Electrochim. Acta 38 (1993) 935.
[5] W.B. Gu, C.Y. Wang, B.Y. Liaw, J. Electrochem. Soc. 144 (1997) 2053.
[6] W.B. Gu, C.Y. Wang, B.Y. Liaw, J. Power Sources 75 (1998) 151.
[7] C.Y. Wang, W.B. Gu, B.Y. Liaw, J. Electrochem. Soc. 145 (1998) 3407.
[8] B.Y. Liaw, K.P. Bethune, X.G. Yang, in: Proceedings of the 200th Electrochemical Society Meetings, San Francisco, CA, 2–7 September 2001 (abstract #71);
B.Y. Liaw, K.P. Bethune, X.G. Yang, in: Proceedings of the Electrochemical Society on Battery Technology and Ultracapacitors, Pennington, NJ.
[9] X.G. Yang, K. P. Bethune, B.Y. Liaw, in: Proceedings of the 200th Electrochemical Society Meetings, San Francisco, CA, 2–7 September 2001 (abstract #67);
X.G. Yang, K. P. Bethune, B.Y. Liaw, in: Proceedings of the Electrochemical Society on Battery Technology and Ultracapacitors, Pennington, NJ.
[10] X.G. Yang, B.Y. Liaw, J. Power Sources 102 (2001) 186.
[11] X.G. Yang, B.Y. Liaw, J. Electrochem. Soc. 148 (2001) A1023–A1028.
[12] J. Crank, The Mathematics of Diffusion, Oxford University Press, Oxford, 1957.